SECED 2023 Conference
Earthquake Engineering & Dynamics for a Sustainable Future
14-15 September 2023, Cambridge, UK

ORIENTATION-INDEPENDENT INELASTIC SPECTRAL DISPLACEMENT INTENSITY MEASURES FOR THE RISK ASSESSMENT OF BRIDGES

Savvinos ARISTEIDOU[1] & Gerard J. O'REILLY[2]

Abstract: *A seismic intensity measure (IM) links the seismic hazard and the dynamic response of a structure subjected to ground shaking. The spectral acceleration at the first and usually dominant vibration mode, $Sa(T_1)$, is a popular choice for building structures. However, the IM selection for bridges is non-trivial since they do not typically have a single dominant mode. Even for ordinary bridges with a dominant mode, the behaviour can change significantly in each direction, but also the non-linear behaviour and components' response varies remarkably from bridge to bridge. This study examines the performance of a novel IM in this context: the nn^{th} percentile of all rotation angles of the inelastic spectral displacement, $Sd_{i,RotDnn}$. This evaluation is carried out within the context of the seismic risk assessment of an ordinary bridge structure. It is compared with other conventional IMs used in regional bridge assessment. The case study bridge is a highway overcrossing located in California with two spans and a continuous prestressed reinforced concrete box girder. A large ground motion set was selected from the NGA-West2 database, and incremental dynamic analysis was performed on the structure to assess each IM's efficiency. Also, different horizontal component definitions were examined in terms of their efficiency. From the results, it can be concluded that $Sd_{i,RotDnn}$ performs very well compared to other IMs. It is also shown that this IM could be a good choice to relate the shaking intensity to the inelastic response that a bridge structure is expected to undergo.*

Introduction

Bridges as part of road networks in seismically prone areas, provide critical lifelines during substantial seismic events in addition to their fundamental role in the daily operation of society. Therefore, it is essential to maintain their serviceability under a wide range of earthquake intensities. While direct monetary losses can be significant, indirect losses, such as expected downtime, often contribute the most to the overall losses (Kilanitis and Sextos, 2019). That is why the assessment of the bridge network resilience in a regional scale can be more impactful and insightful. Nevertheless, many important conclusions can also be drawn from a single bridge seismic assessment.

Within the seismic risk evaluation of a structure, fragility functions are employed to express the probability of the structure being in different levels of damage versus the seismic shaking intensity. One of the key components of fragility functions is the intensity measure (IM), which is a scalar value that connects the level (or intensity) of ground shaking to the structure's performance. Thus, making it an inseparable link within the performance-based earthquake engineering (PBEE) framework (Cornell and Krawinkler, 2000), and should be chosen wisely depending on the type of structures and underlying seismic hazard conditions in hand.

For bridge structures, peak ground acceleration (*PGA*) and spectral acceleration-based, *Sa*(*T*), IMs have traditionally been popular (Borzi et al., 2015). Still, it was suggested (Huang, Gardoni and Hurlebaus, 2010) that peak ground velocity (PGV) may also be pertinent. Recent research has explored the potential of using inelastic spectral displacement as an IM (Wu, Li and Wang, 2019). This approach seeks to more accurately capture the displacement experienced by the structure via a single-degree-of-freedom (SDOF) proxy structure during an earthquake. Inelastic deformations are strongly associated with damage in the piers, such as permanent cracking,

[1] PhD candidate, Scuola Universitaria Superiore IUSS Pavia, Pavia, Italy, savvinos.aristeidou@iusspavia.it
[2] Assistant Professor, Scuola Universitaria Superiore IUSS Pavia, Pavia, Italy

concrete spalling, fracture or buckling of reinforcing bars, or crushing of the core concrete due to fracture of the confining reinforcement, especially in first-mode dominated structures (Tothong and Cornell, 2006). Hence, the hypothesis tested in this paper is that the newly developed

$Sd_{i,RotDnn}$, for which a ground motion model (GMM) was also proposed (Aristeidou, Tarbali and O'Reilly, 2023), could be an excellent means to estimate inelastic deformation and damage in bridge structures accurately. This IM is defined as the inelastic displacement of a SDOF system with bilinear hysteretic behaviour with 3% positive strain hardening ratio and 5%-tangent-stiffness proportional damping. Regarding its horizontal component definition, the Sd_i was calculated for a range of non-redundant rotation angles, with the final output being the 50th and 100th percentile, along with the geometric mean of the two as-recorded orientations. The only inputs of this IM are the initial elastic period, T and the strength ratio, R.

The horizontal component definition can be important, especially when the directionality effect of ground motions is of interest. IMs that incorporate spectral values from both horizontal components of ground motion, e.g., their geometric mean, or better yet from all the possible rotation angles in the horizontal plane, e.g., *RotD50*, have the advantage of removing the sensor orientation as a contributor to epistemic uncertainty (Boore, Watson-Lamprey and Abrahamson, 2006).

This study examines the performance of inelastic spectral displacement using the *RotD50* and *RotD100* component definitions on a case study bridge structure. The results will be compared to those obtained using other traditional and contemporary IMs, in terms of their efficiency. This research contributes to a better understanding of the most appropriate IMs for bridge structures and the relevance of the *RotDnn* component definition in reducing the record-to-record variability.

Case study bridge structure and numerical modelling

To illustrate the relative performance of these novel IMs for bridges, a case study structure was numerically modelled and analysed for the comparisons. The structure adopted in this study was an existing bridge in California constructed in 2001. This bridge is the Jack Tone Road On-Ramp Overcrossing and has been used in past studies (e.g., Fayaz, Dabaghi and Zareian, 2020). It is used here as a reference structure since a good deal of technical documentation is available to allow its sufficiently detailed numerical modelling. It falls under the ordinary reinforced concrete bridge typology, with seat-type abutments, single-pier bent and box-girder deck. A threedimensional finite-element spine model was developed using the open-source software OpenSeesPy (Zhu, McKenna and Scott, 2018). Figure 1 depicts a schematic representation of the three-dimensional finite element model.

Since the bridge's superstructure is designed to remain elastic during earthquake-induced ground shaking, the deck was modelled with an *elasticBeamColumn* element in OpenSeesPy, with gross cross-sectional properties (i.e., $I_{eff} = I_g$), as recommended by Caltrans SDC (2010). The mass of the superstructure was modelled as a consistent distributed mass acting on the pier element and deck elements, with each bridge span discretised into ten deck elements. The bridge pier was modelled using the *forceBeamColumn* element, with fibre-based cross-sections, employing the *HingeRadau* integration method (Scott and Fenves, 2006). The pier was assumed to be fixed at the base for simplicity and monolithically connected to the underside of the deck. Confined and unconfined concrete fibres were modelled using the *Concrete01* uniaxial material model, and the steel rebars were represented using the *Steel02* (i.e., Giuffre-Menegotto-Pinto) material model. The plasticity in the pier element was concentrated at the two ends, which were connected by a linear elastic element with effective cross-section stiffness properties. The shear and torsional behaviour of the pier was modelled elastically using a section aggregator, with the suggested stiffness reduction factors given in the report of Kaviani *et al.* (2014). These were modelled as elastic since failure modes of this type are not expected to occur given the compliance of the case-study bridge with modern seismic design practices. The pier, pier cap and deck are constructed integrally, so a beam-type rigid link was assigned to connect the top end of the pier to the deck element.

For what concerns the bridge ends, a simplified abutment model was adopted, where only three components were explicitly considered: (1) longitudinal response of the backfill (passive pressure) and the expansion joint; (2) transverse response of the shear keys; and (3) vertical response of the bearing pads and the stem wall. The remaining abutment components were omitted, as their contributions to the overall response have been found to be insignificant (Kaviani *et al.*, 2014).

Regarding the longitudinal behaviour of the abutment, five springs were assigned along the deck width, all connected to a rigid beam. The soil backfill response was modelled using the *HyperbolicGapMaterial*. The strength and initial stiffness of the soil springs were obtained from the recommendations provided in Caltrans SDC (2010), which in turn were derived from a largescale abutment testing (Romstad *et al.*, 1995; Stewart *et al.*, 2007). Regarding the transversal behaviour of the abutment, one spring was assigned to each abutment end. It was assumed that the abutment backwall does not contribute significantly to the longitudinal load-bearing capacity of the abutment, since it fails through a brittle mechanism. Regarding the bearing pads, they were assumed to be frictionless. Thus, their transverse and longitudinal shear capacities, and generally their interaction with the deck were disregarded, except in the vertical direction. The shear keys at the deck ends were modelled using macro-elements that resist only in compression and the *Concrete02* hysteretic force-deformation model was assigned (Omrani *et al.*, 2017). This hysteretic model was chosen to avoid convergence problems and solve the simultaneous parallel force balance problem by defining a small strength in tension. Further details about this bridge's characteristics and modelling assumptions are given in the 'Bridge A' description of Kaviani et al. (2014). With regards to damping, a 5%-tangent-stiffness proportional damping model was applied, at the first mode period (Petrini *et al.*, 2008).

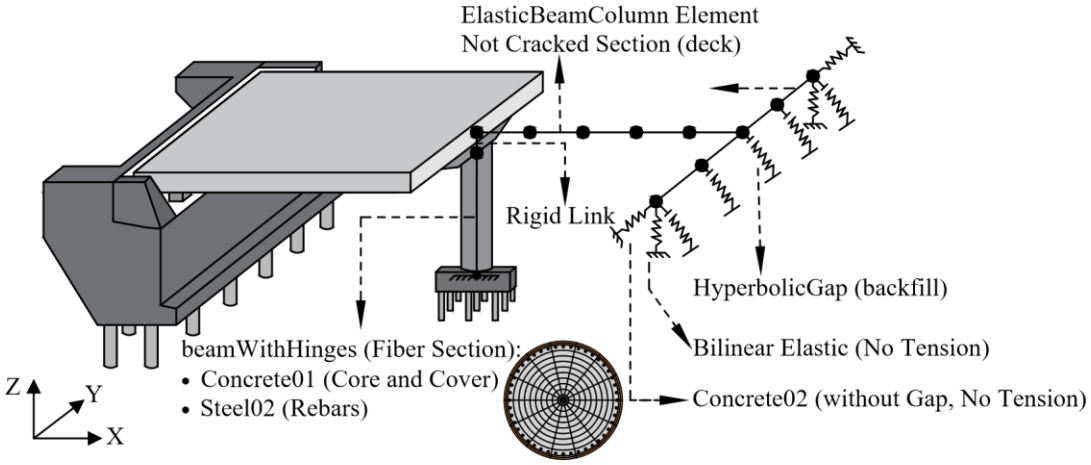

Figure 1. Illustration of the numerical modelling strategy adopted for the case study bridge

Modal analysis was carried out on the bridge model and the first four modes' periods of vibration and their participating mass in each of the principal directions are listed in Table 1. As can be observed through the translational and rotational modal participation factors, *M* and *R*, respectively, the first two modes are primarily in the X direction, with a small rotation component about the Y axis. It should be noted that these modal properties also closely match those reported by Kaviani *et al.* (2014) for the same bridge typology, therefore giving confidence to the accuracy and representativeness of the case study bridge model.

Mode	Period [sec]	Modal participation mass ratios (%)					
		M_X	M_Y	M_Z	R_X	R_Y	R_Z
1	0.604	48.5	0	0	0	31.1	0
2	0.363	50.5	0	0	0	34.6	0
3	0.352	0	88.3	0	0.5	0	0
4	0.336	0	0	75.4	0	0	0

Table 1. Modal analysis results of the case study bridge

Ground motion records

To analyse the seismic performance of the bridge model, incremental dynamic analysis (IDA) (Vamvatsikos and Cornell, 2002) was performed to characterise the non-linear dynamic response of the bridge model right up to lateral collapse. To do this, a sufficiently large set of suitable ground motion records was needed to characterise the structure's seismic response adequately and to

ensure an accurate marginal distribution of IM for a given engineering demand parameter (EDP) threshold (i.e., fragility curves). A set of 200 unscaled ground motion records were selected from the NGA West2 database (Ancheta *et al.*, 2013) based on a scenario of magnitude, M_w = 7.5±0.5, rupture distance, R_{rup} = 20±20 km and soil conditions, $V_{s,30}$ = 400±300 m/s. This relatively large number of ground motions was chosen so that the accuracy of seismic demand estimates does not affect the final results and conclusions, an issue that has been studied in the past by Sousa et al. (2016), for example. Also, a quite intense scenario was chosen to minimise the level of scaling required to bring the structure to its collapse limit. This was especially the case since the bridge under consideration was well-designed against seismic actions. It should be noted that only the horizontal components of the ground motions were applied to the structure as the bridge was not expected to be susceptible to adverse vertical ground-motion effects. Regarding the application of the ground motion records to the structure, the 1st as-recorded component in the NGA-West2 database was applied to the X (longitudinal) direction of the bridge and the 2nd asrecorded component was applied in the Y (transversal) direction. This was kept constant throughout the analysis since past work (Giannopoulos and Vamvatsikos, 2018) has shown that using an adequately large set of ground motion records is more important and produces more reliable results than a smaller set with varying orientation of each individual ground motion record.

Intensity measures

As Bradley (2012) and others have shown, an IM is the interface variable connecting seismological and structural aspects in seismic risk analysis. Seismologists employ seismic hazard analysis to determine the probability of exceeding an intensity level for a certain site over a given period of time. Engineers then utilise this IM to examine the structural response and determine the seismic risk performance of a structure. This characterisation of the interface IM between seismology and engineering is meant to avoid associating the structural response to rupture parameters, *rup*, such as magnitude and distance, condensing all pertinent information in the chosen IM for engineering evaluation. To achieve this disassociation of structural response to *rup* parameters to the highest degree possible, the IM needs to be (i) practical in its predictability via GMMs in hazard analysis, (ii) efficient in its prediction of structural response, (iii) sufficient with respect to the underlying seismic hazard and site characteristics and (iv) unbiased with respect to other ground motion parameters and IMs. In this paper, only the relative efficiency is presented and critically discussed.

Efficiency means that the structural response, measured by an EDP, should exhibit minimal record-to-record variability at any given level of the IM, or reversely, low IM level variability at any given structural response (i.e., EDP) level. This IM attribute allows one to accurately evaluate the conditional EDP distribution with relatively few response-history analyses. This can become important when conducting a plethora of non-linear dynamic analyses for a building class portfolio, or in regional assessment. However, it is worth noting that within a risk assessment framework, like the PEER-PBEE framework (Cornell and Krawinkler, 2000), this reduction in response dispersion gained by a more efficient IM, does not necessarily reduce the overall dispersion. A more efficient IM may be more structure-specific and, therefore, present lower dispersion in predicting the structural response, but this may come at the cost of higher dispersions from the GMM.

Several studies have focused on investigating IM performance in bridge structures (Mehdizadeh, Mackie and Nielson, 2017; Monteiro *et al.*, 2019; O'Reilly, 2021) but are typically related to spectral acceleration-based or velocity-based IMs. However, none of these studies has so far examined the relative performance of inelastic spectral displacement-based IMs, which have been the focus of recent research (Ruiz-García and Miranda, 2007; Aristeidou, Tarbali and O'Reilly, 2023; Bahrampouri *et al.*, 2023). Also, the issues of directionality are worth exploring for what concerns bridge structures and are thus examined further here. Based on the above considerations and also the need to address the ground motion directionality effects on bridge structures, the following intensity measures were investigated and are defined as follows:

- *PGA*: peak ground acceleration;
- *PGV*: peak ground velocity;
- *PGD*: peak ground displacement;
- $Sa(T_1)$: 5%-damped spectral acceleration at the fundamental period, T_1, of the case-study structure;
- $Sd_{i,RotDnn}$: 5%-tangent-stiffness damped inelastic spectral displacement, where two *RotDnn* definitions were considered: the 50th and 100th percentile of all rotation angles sorted by amplitude (i.e., *RotD50* and *RotD100*) as defined by Boore (2010);

- *FIV3*: filtered incremental velocity, as defined by Dávalos and Miranda (2019) and Eq. (2);
- *AvgSa*: average spectral acceleration as defined by Eq. (1), which was further subdivided according to the period range for a subsequent parametric study as follows:
    - *AvgSa1* – $T \in [0.5T_1, 1.5T_1]$
    - *AvgSa2* – $T \in [0.5T_1, 2T_1]$
    - *AvgSa3* – $T \in [0.5T_1, 3T_1]$

Average spectral acceleration, *AvgSa*, is defined as the geometric mean of *N*-number spectral accelerations at periods within a user-specified range [T_{lower}, T_{upper}], expressed as in Eq. (1). Herein, ten periods (i.e., *N*=10) equally spanning each chosen period range were used.

$$AvgSa = [\prod_{i=1}^{N} Sa(T_i)]^{1/N} \qquad \text{for } T \in [T_{lower}, T_{upper}] \tag{1}$$

The filtered incremental velocity, *FIV3*, is defined as follows:

$$FIV3 = \max\{V_{s,max1} + V_{s,max2} + V_{s,max3}, |V_{s,min1} + V_{s,min2} + V_{s,min3}|\} \tag{2}$$

$$V_s(t) = \{\int_{t}^{t+\propto \cdot Tn} \ddot{u}_{gf}(\tau)d\tau, \ \ \forall t < t_{end} - \propto \cdot T_n\} \tag{3}$$

where, $V_s(t)$ is a series of incremental velocities, *IVs*, computed using time segments with duration $\alpha \cdot T_n$, $V_{s,max1}$, $V_{s,max2}$, and $V_{s,max3}$, are the three local largest *IVs* in $V_s(t)$, and similarly $V_{s,min1}$, $V_{s,min2}$, and $V_{s,min3}$, are the three local minimum *IVs* in $V_s(t)$, T_n corresponds to the fundamental period of vibration of the structure, t_{end} corresponds to the last instant of time of the acceleration time series, and $\ddot{u}_{gf}$ corresponds to the filtered acceleration time series using a second-order Butterworth lowpass filter with a cut-off frequency, f_c, equal to $\beta \cdot f_n$, where β is a scalar input that controls the f_c/f_n ratio. The α and β input parameters required to calculate Eq. (2) were chosen as 0.7 and T_n, respectively, as recommended by Dávalos and Miranda (2020), since after a parametric analysis on a set of seven moment resisting frame structures they found that small departures from optimum values did not increase significantly the variability of collapse intensities.

Analysis results

Using the set of 200 ground motion records described in precious section, IDA was performed in order to quantify the full response of the bridge structure up to collapse. For computational efficiency, this was done using the hunt and trace algorithm described in Vamvatsikos and Cornell (2002). The EDP chosen was the pier drift, and the IDA was conducted until a pier drift of 10%. The curves are plotted until 6% drift, as this was the value at which the pier began to lose lateral strength capacity, as determined from a pushover analysis of the pier element. The IDA was initially conducted using $Sa(T_1)$ as the IM, as shown in Figure 2, and the IDA curves for the other aforementioned IMs were obtained by simple post-processing of the analysis results to allow for relative comparisons. Also plotted are the median trend of the response along with the 16th and 84th percentiles to graphically illustrate the variability of the structural response. The general trend of the median is a steady increase with intensity before reaching a plateau (i.e., flatline), where the structure is considered to be collapsed. It can be seen that the IM dispersion is relatively low initially and gradually increases. This dispersion is mainly a combined consequence of the recordto-record variability of the ground motions, the IM used and the multi-modal behaviour of the inelastically responding structure. The response may also be examined in terms of alternative EDPs, such as the longitudinal and transversal response of the abutment system, or bearings and shear keys response. However, these were not judged to be principal elements to examine for the present study.

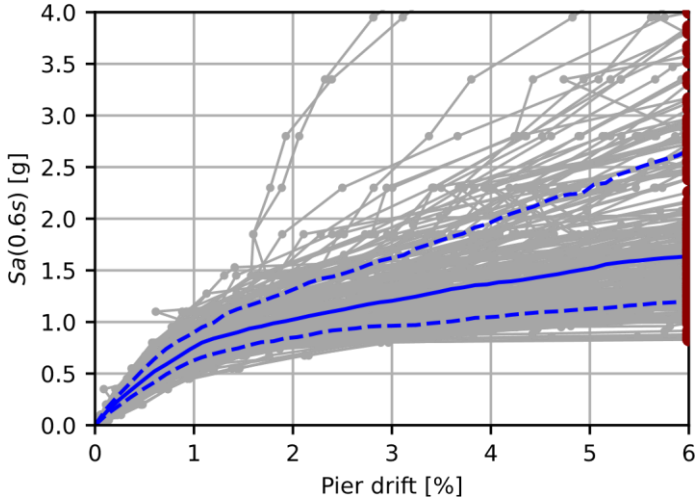

Figure 2. IDA curves of the 200 GMs along with the 16, 50 and 84 percentiles

Efficiency

Considering the IDA response in Figure 2 for the case study bridge structure, the efficiency of the IMs was examined. This was done by comparing the dispersions in the results to evaluate each IM's predictive power. A principal assumption is that the data shown in Figure 2 are lognormally distributed and characterised by a median and dispersion value pair, $\{\eta, \beta\}$. For the present study, the dispersion of IM at a given EDP, $\beta_{IM|EDP}$, also known as record-to-record variability, β_{RTR}, was computed for each IM examined over the whole EDP range. The dispersions for each IM described previously were computed and are depicted in Figure 3. Also shown is the corresponding pier displacement ductility, μ_Δ, where it can be seen that a ductility well over 8 was obtained before the lateral collapse of the pier element.

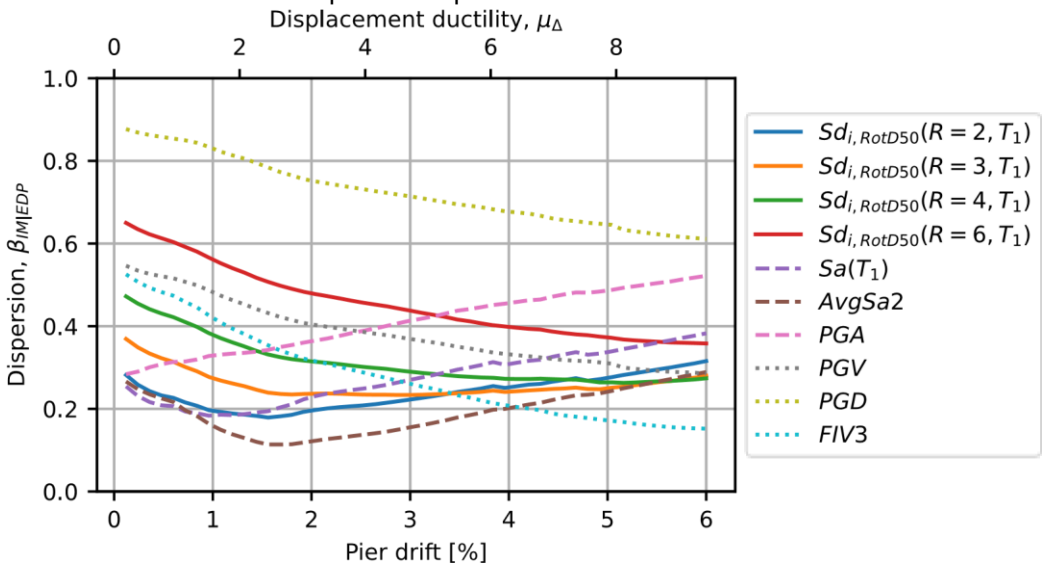

Figure 3. Intensity measure dispersion versus pier drift and displacement ductility for each IM investigated. For visual clarity different line styles were used according to the IM category. $Sd_{i,RotD50}$ IMs: solid line; acceleration-based IMs: dashed line; other IMs: dotted line.

Beginning with the spectral acceleration, $Sa(T_1)$, it can be seen how it gives relatively low dispersion in the elastic range (i.e., $\mu_\Delta \leq 1$) and close to that region, but the dispersion increases as the structure goes deeper into the non-linear range of response. This is an expected result for any structure since past studies (Bradley *et al.*, 2009; Lin, Haselton and Baker, 2013) have shown that $Sa(T_1)$ is well correlated with deformation-based EDPs only for first-mode-dominant structures that stay in or near the elastic range of response. *PGD* exhibits the highest $\beta_{IM|EDP}$ throughout the whole range of structural response, whereas *PGA* is also seen to increase progressively, making them the worst performers among all IMs.

Meanwhile, in the region with a highly inelastic response and near the collapse limit it is the *FIV3* which performs the best. The findings of the original study (Dávalos and Miranda, 2019) proposing the use of latter IM are further supported by the results observed in this study. Specifically, this IM has demonstrated the highest efficiency in predicting the seismic collapse intensities of the structure, as evidenced by the smallest record-to-record variability. This effect of FIV3 is because, unlike other IMs based on the peak response of one or more linear elastic oscillators, it is defined based on features of severe long-duration acceleration pulses present in the acceleration time series, which are deemed to be the main drivers of collapse.

Among the novel $Sd_{i,RotD50}$ definitions, the most efficient for pier drifts lower than about 3% is the one with R = 2, whereas for drifts higher than 3% R = 3 performs better. This is expected since the force reduction factor of the SDOF, with which $Sd_{i,RotD50}$ was developed, is a proxy of the inelasticity that the system is expected to undergo. Ergo, a higher R corresponds to higher efficiency in the high EDP region.

The dispersion of the three definitions of *AvgSa* investigated was calculated and plotted in Figure 4 for the whole range of non-linear response. The lower bound of the period range was kept the same since it was seen that the dispersion was already low enough for low EDP values. It can be seen that *AvgSa1* performs the best for pier drifts until about 1.3%, then for drifts of 1.3-2.3%, the *AvgSa2* is the most efficient and from there until 6% drift the *AvgSa3* has the best performance. This is expected since the upper bound of the period range accounts for the effects of period elongation during non-linear response. Therefore, the structural response deep into the non-linear range is better explained using a higher T_{upper}. Taking *AvgSa2* to be the best overall performer for the case study presented here, it can be seen from Figure 3 that it is the most efficient IM in the initial elastic region and, most evidently, in the intermediate inelastic region.

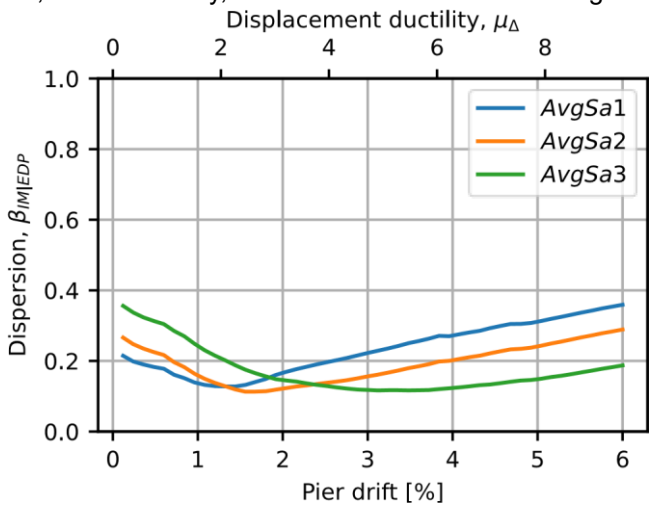

Figure 4. Marginal dispersion of AvgSa with different period ranges

From these observations, it is clear that the choice of IM depends on which part of the structural response is of interest, as no single IM produces the overall best efficiency. For instance, if an inefficient IM, such as *PGD*, *PGA*, or $Sa(T_1)$, is chosen to estimate the IM at the collapse limit state, it will result in high dispersion in the results and require many more GM records to characterise the collapse fragility sufficiently. However, some of these IMs work better at limit states other than collapse. The inelastic spectral displacement definitions have shown promising performance as IMs, with comparable, if not better, efficiency with respect to other notable IMs currently in use.

Comparison of different horizontal component definitions

While the previous section looked at the relative efficiency of the different IMs, this section looks at the impacts the horizontal component definition can have on the results. The efficiency of two horizontal component definitions of elastic spectral accelerations and inelastic spectral displacements were examined in this respect. The results of the relative comparison are shown in Figure 5.

It is seen that the dispersion in the *RotD100* component definition of the $Sa(T)$ is around 8.1% higher on average than the *RotD50* component. This is a somewhat expected result when considering the actual definition of these IMs: the *RotD50* component is the median over all

directions; hence, it has a more averaging effect and does not suffer peaks as much as the *RotD100* component does, which takes the maximum over all directions. The same observation is also noted for the *AvgSa* shown in Figure 5(a), but with a less amplified effect as it is only 2.9% higher on average, because of the further averaging effect of *AvgSa* over the predefined period range.

Regarding the inelastic spectral displacements, Sd_i, the same general trend is observed as in the case of the elastic IMs, which is conceptually consistent. However, it is worth noting that the ratio of the dispersions between the *RotD100* and *RotD50* definitions is larger, around 17.3% on average. This is because in the Sd_i the non-linear cycles produce a maximum displacement that can accumulate more in the non-linear range, especially along the *RotD100* orientation; hence, the maximum with respect to the median definitions can tend to deviate more, as observed in Figure 5(b). From a visual inspection of Figure 5(b), this may be the case, but no significant trend is noted, as the average ratios are 10.7%, 23.3%, 22.2% and 13.0% for the R = 2, 3, 4 and 6 cases, respectively. Strangely enough, the highest ratios of dispersion of the two horizontal component definitions are observed for the intermediate R factors, hence there is not an evident trend among the different Sd_i definitions.

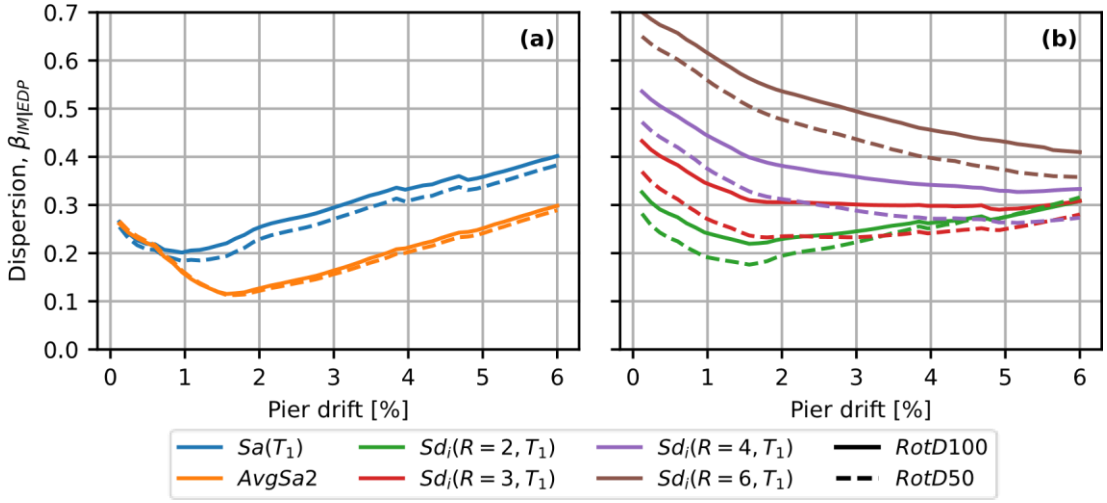

Figure 5. Comparison of dispersion for different horizontal component definitions (a) elastic spectral accelerations and (b) inelastic spectral displacements

Summary and conclusions

This paper has investigated the use of orientation-independent inelastic spectral displacements, $Sd_{i,RotDnn}$, as an intensity measure (IM) for seismic assessment of a case study bridge structure. A typical reinforced concrete highway bridge in California was employed for the comparisons. Its dynamic response up to collapse was characterised versus the ground shaking intensity. Assorted traditional and contemporary IMs were examined and compared on the basis of their efficiency to characterise the structural response. Based on the outcomes of this study, the following conclusion can be drawn out:

- The novel IM $Sd_{i,RotD50}$ performed relatively well in predicting the EDP against the efficiency checks. An interesting and expected result is that the efficiency of Sd_i with different force reduction factors, R, varies with the level of inelasticity. Specifically, for low R factors, the lowest dispersions are found in the elastic or early inelastic ranges, whereas for the higher R factors, the lowest dispersion is found deeper into the inelastic range or near the collapse limit;
- The *RotD100* component falls short of predicting the resultant pier drift response compared to the *RotD50* component. This is the case for both elastic and inelastic spectral values, with the effect on inelastic spectral values being more amplified;
- For the biggest range of structural response, it was the *AvgSa2* that was the most efficient (i.e., displayed the lowest dispersion). Meanwhile, near and at collapse limit the *FIV3* performed the best;

- It was briefly shown how the period range used to define *AvgSa* can have a significant impact. It should be chosen carefully, based on what level of inelastic response one wants to have the best control over.

Acknowledgements

The work presented in this paper has been developed within the framework of the project "Dipartimenti di Eccellenza", funded by the Italian Ministry of Education, University and Research at IUSS Pavia.

References

Ancheta, T. *et al.* (2013) 'PEER NGA-West2 Database, Technical Report PEER 2013/03'.

Aristeidou, S., Tarbali, K. and O'Reilly, G.J. (2023) 'A ground motion model for orientationindependent inelastic spectral displacements from shallow crustal earthquakes', *Earthquake Spectra*, 0(0), pp. 1–23. Available at: https://doi.org/10.1177/87552930231180228.

Bahrampouri, M. *et al.* (2023) *Use of Inelastic Response Spectra in Seismic Hazard Analysis and Design*. Available at: https://doi.org/10.34948/N38G6K.

Boore, D.M. (2010) 'Orientation-independent, nongeometric-mean measures of seismic intensity from two horizontal components of motion', *Bulletin of the Seismological Society of America*, 100(4), pp. 1830–1835. Available at: https://doi.org/10.1785/0120090400.

Boore, D.M., Watson-Lamprey, J. and Abrahamson, N.A. (2006) 'Orientation-independent measures of ground motion', *Bulletin of the Seismological Society of America*, 96(4 A), pp. 1502–1511. Available at: https://doi.org/10.1785/0120050209.

Borzi, B. *et al.* (2015) 'Seismic Vulnerability of the Italian Roadway Bridge Stock', *Earthquake Spectra*, 31(4), pp. 2137–2161. Available at: https://doi.org/10.1193/070413EQS190M.

Bradley, B.A. *et al.* (2009) 'Prediction of spatially distributed seismic demands in specific structures: Ground motion and structural response', *Earthquake Engineering & Structural Dynamics*, 39, pp. 501–520. Available at: https://doi.org/10.1002/eqe.954.

Bradley, B.A. (2012) 'The seismic demand hazard and importance of the conditioning intensity measure', *Earthquake Engineering & Structural Dynamics*, 41(11), pp. 1417–1437. Available at: https://doi.org/10.1002/eqe.2221.

Caltrans (2010) *Caltrans Seismic Design Criteria Version 1.6. California Department of Transportation*. Sacramento, CA.

Cornell, C.A. and Krawinkler, H. (2000) 'Progress and challenges in seismic performance assessment', *PEER Center News*, 3(2), pp. 1–2.

Dávalos, H. and Miranda, E. (2019) 'Filtered incremental velocity: A novel approach in intensity measures for seismic collapse estimation', *Earthquake Engineering and Structural Dynamics*, 48(12), pp. 1384–1405. Available at: https://doi.org/10.1002/eqe.3205.

Dávalos, H. and Miranda, E. (2020) 'Evaluation of FIV3 as an Intensity Measure for Collapse Estimation of Moment-Resisting Frame Buildings', *Journal of Structural Engineering*, 146(10), pp. 1–14. Available at: https://doi.org/10.1061/(asce)st.1943-541x.0002781.

Fayaz, J., Dabaghi, M. and Zareian, F. (2020) 'Utilization of Site-Based Simulated Ground Motions for Hazard-Targeted Seismic Demand Estimation: Application for Ordinary Bridges in Southern California', *Journal of Bridge Engineering*, 25(11). Available at: https://doi.org/10.1061/(asce)be.1943-5592.0001634.

Giannopoulos, D. and Vamvatsikos, D. (2018) 'Ground motion records for seismic performance assessment: To rotate or not to rotate?', *Earthquake Engineering and Structural Dynamics*, 47(12), pp. 2410–2425. Available at: https://doi.org/10.1002/eqe.3090.

Huang, Q., Gardoni, P. and Hurlebaus, S. (2010) 'Probabilistic Seismic Demand Models and Fragility Estimates for Reinforced Concrete Highway Bridges with One Single-Column Bent', *Journal of Engineering Mechanics*, 136(11), pp. 1340–1353. Available at: https://doi.org/10.1061/(ASCE)EM.1943-7889.0000186.

Kaviani, P., Zareian, F. and Taciroglu, E. (2014) *Performance-Based Seismic Assessment of Skewed Bridges*, *Pacific Earthquake Engineering Research Center (PEER)*. Available at: https://doi.org/10.13140/2.1.1586.0007.

Kilanitis, I. and Sextos, A. (2019) 'Impact of earthquake-induced bridge damage and time evolving traffic demand on the road network resilience', *Journal of Traffic and Transportation Engineering (English Edition)*, 6(1), pp. 35–48. Available at: https://doi.org/10.1016/j.jtte.2018.07.002.

Lin, T., Haselton, C.B. and Baker, J.W. (2013) 'Conditional spectrum-based ground motion selection. Part II: Intensity-based assessments and evaluation of alternative target spectra', *Earthquake Engineering & Structural Dynamics*, 42(12), pp. 1867–1884. Available at: https://doi.org/10.1002/eqe.2303.

Mehdizadeh, M., Mackie, K.R. and Nielson, B.G. (2017) 'Scaling Bias and Record Selection for Quantifying Seismic Structural Demand', *Journal of Structural Engineering*, 143(9), pp. 1–12. Available at: https://doi.org/10.1061/(asce)st.1943-541x.0001855.

Monteiro, R. *et al.* (2019) 'Derivation of Fragility Functions for Seismic Assessment of RC Bridge Portfolios Using Different Intensity Measures', *Journal of Earthquake Engineering*, 23(10), pp. 1678–1694. Available at: https://doi.org/10.1080/13632469.2017.1387188.

O'Reilly, G.J. (2021) 'Seismic intensity measures for risk assessment of bridges', *Bulletin of Earthquake Engineering*, 19(9), pp. 3671–3699. Available at: https://doi.org/10.1007/s10518-021-01114-z.

Omrani, R. *et al.* (2017) 'Variability in the predicted seismic performance of a typical seat-type California bridge due to epistemic uncertainties in its abutment backfill and shear-key models', *Engineering Structures*, 148, pp. 718–738. Available at: https://doi.org/10.1016/j.engstruct.2017.07.018.

Petrini, L. *et al.* (2008) 'Experimental verification of viscous damping modeling for inelastic time history analyzes', *Journal of Earthquake Engineering*, 12(SUPPL. 1), pp. 125–145. Available at: https://doi.org/10.1080/13632460801925822.

Romstad, K.M. *et al.* (1995) *Experimental measurements of bridge abutment behavior. Report No. UCD STR 95 1*. University of California, Structural Engineering Group, Davis, CA.

Ruiz-García, J. and Miranda, E. (2007) 'Probabilistic estimation of maximum inelastic displacement demands for performance-based design', *Earthquake Engineering and Structural Dynamics*, 36(9), pp. 1235–1254. Available at: https://doi.org/10.1002/eqe.680.

Scott, M.H. and Fenves, G.L. (2006) 'Plastic Hinge Integration Methods for Force-Based Beam–Column Elements', *Journal of Structural Engineering*, 132(2), pp. 244–252. Available at: https://doi.org/10.1061/(asce)0733-9445(2006)132:2(244).

Sousa, L. *et al.* (2016) 'On the treatment of uncertainties in the development of fragility functions for earthquake loss estimation of building portfolios', *Earthquake Engineering & Structural Dynamics*, 45(12), pp. 1955–1976. Available at: https://doi.org/10.1002/eqe.2734.

Stewart, J. *et al.* (2007) *Full Scale Cyclic Testing of Foundation Support Systems for Highway Bridges. Part II : Abutment Backwalls. Report No. UCLA SGEL 2007/02*. University of California, Los Angeles, CA.

Tothong, P. and Cornell, C.A. (2006) 'An empirical ground-motion attenuation relation for inelastic spectral displacement', *Bulletin of the Seismological Society of America*, 96(6), pp. 2146–2164. Available at: https://doi.org/10.1785/0120060018.

Vamvatsikos, D. and Cornell, C.A. (2002) 'Incremental dynamic analysis', *Earthquake Engineering and Structural Dynamics*, 31(3), pp. 491–514. Available at: https://doi.org/10.1002/eqe.141.

Wu, Y.F., Li, A.Q. and Wang, H. (2019) 'Inelastic displacement spectra for Chinese highway bridges characterized by single-degree-of-freedom bilinear systems', *Advances in Structural Engineering*, 22(14), pp. 3066–3085. Available at: https://doi.org/10.1177/1369433219857845.

Zhu, M., McKenna, F. and Scott, M.H. (2018) 'OpenSeesPy: Python library for the OpenSees finite element framework', *SoftwareX*, 7, pp. 6–11. Available at: https://doi.org/10.1016/j.softx.2017.10.009.